

Detection of pore space in CT soil images using artificial neural networks

M. G. Cortina-Januchs^{1,2}, J. Quintanilla-Dominguez^{1,2}, A. Vega-Corona², A.M. Tarquis¹ and D. Andina¹

[1]{Technical University of Madrid, Madrid, Spain}

[2]{University of Guanajuato, Guanajuato, Mexico}

Correspondence to: M.G. Cortina-Januchs (januchs@salamanca.ugto.mx)

Abstract

Computed Tomography (CT) images provide a non-invasive alternative for observing soil structures, particularly pore space. Pore space in soil data indicates empty or free space in the sense that no material is present there except fluids such as air, water, and gas. Fluid transport depends on where pore spaces are located in the soil, and for this reason, it is important to identify pore zones. The low contrast between soil and pore space in CT images presents a problem with respect to pore quantification. In this paper, we present a methodology that integrates image processing, clustering techniques and artificial neural networks, in order to classify pore space in soil images. Image processing was used for the feature extraction of images. Three clustering algorithms were implemented (K-means, Fuzzy C-means, and Self Organizing Maps) to segment images. The objective of clustering process is to find pixel groups of a similar grey level intensity and to organise them into more or less homogeneous groups. The segmented images are used for test a classifier. An Artificial Neural Network is characterised by a great degree of modularity and flexibility, and it is very efficient for large-scale and generic pattern recognition applications. For these reasons, an Artificial Neural Network was used to classify soil images into two classes (pore space and solid soil). Our methodology shows an alternative way to detect solid soil and pore space in CT images. The percentages of correct classifications of pore space of the total number of classifications among the tested images were 97.01 %, 96.47 % and 96.12%.

1 1 Introduction

2

3 Soil structure describes the arrangement of the solid parts of the soil and the pore space
4 located between them. Soil structure is dependent upon the material it is derived from, the
5 environmental conditions under which the soil formed, the amount of clay present and the
6 organic materials present. Pore space is the portion of the soil volume that is not occupied by
7 solid soil but rather by air and/or water. Soil texture, presence of organic matter, the nature of
8 the crops cultivated and soil depth have a great influence on soil pore space. Image analysis of
9 soil has been used for physical and chemical characterisation, macromorphology and
10 micromorphology.

11

12 Several instruments have been used to obtain soil images, such as light microscopes,
13 Scanning Electron Microscopes (SEM), Transmission Electron Microscopes (TEM),
14 Computed Tomography (CT) and Magnetic Resonance Imaging (MRI). In the past few
15 years, geoscientists have started to use CT images of soil for characterising and modelling soil
16 properties. CT images provide a non-invasive alternative for observing soil structure. CT
17 images involve a revolving x-ray tube that surrounds a soil sample and a detector unit to
18 produce 2-D images to provide grey-level images of slices of the sample after computer
19 integration. During this integration process, 3D images are generated (Mermut, 2009). The
20 main issue in CT soil imaging is the low contrast between soil and pore space. Pore space is
21 represented in CT images by dark pixels (0 - grey level), and soil is represented by clear
22 pixels (255- grey level)(Vogel, 1996).

23

24 In general, image analysis involves many different tasks, such as segmentation, classification
25 and interpretation. Segmentation involves identifying objects into images. Classification
26 assigns labels to individual pixels by taking into account previous information on the problem
27 of interest. Interpretation involves extracting some meaning from the image as a whole. The
28 segmentation of soil images is very important for the measurement of properties as well as for
29 detecting and recognising objects in the soil.

30

1 Different methods have been used to segment soil images such as a simple binary threshold
2 method (Perret, 2003) and a multiple threshold method (Pal et al. 1993, Vogel, 1996,
3 Capowiez et al. 1998, Tarquis et al. 2009). Vogel, et al., 1996 suggested using thresholds for
4 typical and critical regions. They calculated a lower limit of the critical region for each
5 individual image as the average of the lower maximum and minimum between the two
6 maxima in the grey-level histogram. Capowiez et al. (1998) used a simple rule to determine
7 the threshold value based on the grey-level histogram. By adding 1/3 of the distance between
8 the pore peak and the matrix peak to the pore peak, they identified the approximate minimum
9 of the distribution function between the two peaks. Pal et al. (1993) suggested local
10 thresholding schemes in which the voxel classification depends on the grey-scale values of its
11 surrounding voxels instead of using global-level values as thresholds. Oh and Lindquist
12 (1999) developed a local threshold method based on the Mardia-Hainsworth spatial
13 thresholding algorithm; details on this method can be found in Mardia and Hainsworth
14 (1988).

15

16 The aim of the present work is to detect pore space in 2D images (that is, axial views)
17 acquired using tomography techniques. The methodology is composed of three steps. The first
18 step is called feature extraction; we applied an erosion morphological operation to enhance
19 the dark regions (pore space). In the next step, three clustering methods were implemented to
20 segment soil images, including (K-means, Fuzzy C-means and Self Organizing Maps). In
21 the last step, an Artificial Neural Network was implemented to classify soil and pore space
22 using the segmented images. Fig. 1 shows the block diagram of our proposed method. Our
23 goal is to obtain an image in which pore and soil spaces can be distinguished.

24

25 **2 Materials and methods**

26 **2.1. Soil image**


27 Soil samples were collected from four horizons of an argissol formed on the Tertiary
28 Barreiras group of formations in Pernambuco, Brazil, at the Itapirema Experimental Station.
29 According to the classification scheme of Köppen, the area has a tropical monsoon climate.
30 The physical and chemical characterisation, macromorphology and micromorphology of this

1 soil have been broadly analysed by Melo and dos Santos (1996). The physical characteristics
2 of the soil are provided in Table 1.

3

4 The intact soil samples were imaged using an EVS MS-MicroCT scanner (now GE Medical,
5 London, Canada). Though some samples required paring to fit into the 64-mm-diameter
6 imaging tubes, the field orientation was maintained. Imaging parameters were 155 keV and
7 25 μ A.

8

9 Proprietary software (GE Medical) was used to reconstruct the 16-bit 3D imagery from the
10 axial sequence views. The resulting voxel size was 45.1 μ A. Accordingly, three sub-volumes
11 were extracted from each of the four original volumes using GE Medical Microview; care was
12 taken to ensure no overlay of the sub-volumes. The sub-volumes measured 256x256x 256
13 units, corresponding to about 16.8 million voxels. A 3D Gaussian filter was also run in
14 Microview (GE Healthcare, 2006) on each sub-volume to reduce noise and beam-hardening
15 artefacts, typically occurs in CT imaging (Tarquis et al., 2009).

16

17 **2.2 Feature extraction**

18 Feature extraction is the process of locating information of interest to detect pore space in soil
19 images. The idea is that feature extraction identifies different features of the same pattern
20 corresponding to different levels of importance and thereby carrying different information.
21 First, an erosion morphological operation was applied to enhance pore areas. Second, spatial
22 domain features were used to obtain information on the neighbourhood of each pixel; in this
23 work, we computed two window-based features (namely, mean and standard deviation) with
24 different window sizes (3x3, 5x5) in the eroded image. In order to select the best size
25 window, we calculated the correlation between the mean and standard deviation for each
26 image.

27

28 Using the extracted features and the grey-level intensity of the original image, a Feature
29 Vector (FV) was constructed. This FV is used for image segmentation. The FV is composed
30 as $\mathbf{x}^{(qs)} = \{[x_1^{(qs)}, x_2^{(qs)}, x_3^{(qs)}, x_4^{(qs)}]\}$, where $q_s = 1, \dots, Q_s$. Note that $Q_s = M \times N$, where $M \times N$ is

1 the image size. $x_1^{(qs)}$ corresponds to the grey-level intensity of the original images. $x_2^{(qs)}$
2 corresponds to the grey level of the eroded image, and $x_3^{(qs)}$ and $x_4^{(qs)}$ correspond to the mean
3 and standard deviation of the eroded image, respectively.

4

5 **2.2.1 Mathematical Morphology**

6 Mathematical Morphology is a discipline in the field of image processing that involves an
7 analysis of the structure of images. Image processing using morphological transformation is a
8 process of information removal based on size and shape. In this process, irrelevant image
9 content is eliminated selectively, and thus the essential image features can be enhanced. Using
10 the concept of structuring elements, intersections and unions in the image with the translations
11 of the structuring element yield two basic morphological operations, namely, erosion and
12 dilation (Gonzalez et al. 2002).

13

14 Erosion generally decreases the size of objects and removes small anomalies by subtracting
15 objects with radii smaller than the given structuring element. With grey-scale images, erosion
16 reduces the brightness (and therefore the size) of bright objects on a dark background using
17 the neighbourhood minimum when shifting the structuring element over the image. Erosion is
18 denoted by

$$19 \quad (I \ominus E)(x, y) = \max[I(x - i, y - j) - E(i, j)], \quad (1)$$

20 where $I(x,y)$ is a grey-scale image, and $E(i,j)$ is the structuring element.

21 In contrast to erosion, dilation generally increases the sizes of objects, fills in holes and
22 broken areas and connects areas that are separated by spaces smaller than the size of the
23 structuring element. With grey-scale images, dilation increases the brightness of objects by
24 taking the neighbourhood maximum when shifting the structuring element over the image.
25 Dilation is denoted by

$$26 \quad (I \oplus E)(x, y) = \min[I(x - i, y - j) + E(i, j)] \quad (2)$$

27 where $I(x,y)$ is a grey-scale image, and $E(i,j)$ is the structuring element.

28

29

1 2.2.2. Spatial domain features

2 Spatial domain features include both shape-related features and window-based features. In
3 this work, we applied window-based features. These features are the mean and standard
4 deviation, which are extracted from images within a rectangular window.

5

$$6 \quad I_{\mu} = \frac{1}{n \times m} \sum_{i=1}^n \sum_{j=1}^m I(i, j) \quad (3)$$

$$7 \quad I_{STD} = \left(\frac{1}{n \times m} \sum_{i=1}^n \sum_{j=1}^m (I(i, j) - I_{\mu})^2 \right)^{1/2}, \quad (4)$$

8 where I_{μ} and I_{STD} represent the mean and standard deviation, respectively, of an image, with
9 $n \times m$ is the window size, I is an image and (i, j) is the pixel position.

10

11 2.3 Image segmentation using clustering techniques

12 Another important role of segmentation in image analysis is in high-level image interpretation
13 and understanding. Segmentation subdivides an image into its constituent regions or objects.
14 The level to which the subdivision is carried out depends on the problem being solved
15 (Gonzalez, et al. 2002). The segmentation of soil images is very important for the
16 measurement of properties as well as for detecting and recognising objects in the soil. The
17 approaches to segmentation proposed in the literature vary depending on the specific
18 application, such as CT or MRI. The main problem in CT soil images is the low contrast
19 between soil and pore space. Pore space is represented in CT images by dark pixels (0 - grey
20 level), and soil is represented by clear pixels (255 - grey level) (Vogel, 1996).

21

22 Tarquis et al. (2009) and Piñuela et al. (2009), used the Peak Fitting Module to analyze the
23 histogram, in order to identification of constituent peaks in the grey-scale histogram. The
24 ~~major~~ peak with the lowest mean digital number was taken to be that corresponding to the
25 pore space; the next major peak was considered to be solid soil, assuming Gaussian
26 distribution for both peaks. In this work, we used clustering techniques based on partitional
27 clustering. Partitional techniques have advantages in applications involving large data sets, for
28 example, soil image data. Soil images present different regions in which the pore and solid

1 mix may hinder the identification of each region. A problem that accompanies the use of a
2 partitional algorithm is the need to choose the number of desired output clusters. We propose
3 and compare three clustering methods to segment soil images (K-Means, Fuzzy c-Means and
4 Self Organising Maps). These clustering methods have been used to segment natural images
5 (Jian, 2004, Lázaro J. et al., 2006, Ye, 2009), satellite images (Chuang, 2006, Arias, 2009)
6 and mammograms images (Vega-Corona ,2003, De Oliveira, 2009, Quintanilla-Dominguez,
7 2009).

8

9 The objective of the clustering process used to segment images is to find pixel groups with a
10 similar grey-level intensity in order to integrate them into homogeneous groups. Similarity is
11 evaluated according to a distance measure between the pixel and the prototypes of the object
12 or region prototypes, and each pixel is assigned to the nearest or most similar prototype.
13 However, this process must distribute all data to the different groups, even if some pixels are
14 not very representative of the group as a whole (Ojeda-Magaña, 2009).

15

16

17 **2.3.1 K-Means algorithm**

18 The K-means algorithm (MacQueen, 1967) is one of the simplest unsupervised learning
19 algorithms that is used to solve the well- known clustering problem. The procedure involves a
20 simple and easy way to classify a given data set into a certain number of clusters (namely, k
21 clusters), which is fixed a priori. The main idea is to define k centroids, that is, one for each
22 cluster. The next step is to take each point belonging to a given data set and associate it with
23 the nearest centroid. When no additional points are available for clustering, the first step is
24 completed, and an early group is done. At this point, we must re-calculate k new centroids at
25 vary centres of the clusters resulting from the previous step. After we obtain these k new
26 centroids, a new binding is conducted between the same data set points and the nearest new
27 centroid. A loop is then generated. Based on this loop, we may notice that the k centroids
28 change their location step by step until no more changes occur, that is, centroids do not move
29 anymore. Finally, this algorithm minimises an objective function, which in this case is a
30 squared error function, as follows:

$$J = \sum_{j=1}^k \sum_{i=1}^n \|x_i^{(j)} - c_j\|^2, \quad (5)$$

where $\|x_j^{(j)} - c_i\|^2$ is the Euclidean distance measure between a data point $x_j^{(j)}$ and the cluster c_j , which serves as an indicator of the distance between the n data points and their cluster centres. The algorithm is composed of the following steps:

- Place k points into the space represented by the objects that are being clustered. These points represent the initial centroids.
- Assign each object to the group with the closest centroid.
- When all objects have been assigned, recalculate the positions of the k centroids.
- Repeat the second and third steps until the centroids no longer move. This produces a separation of the objects into groups from which the metric to be minimised can be calculated.

Although it can be proven that the procedure will always terminate, the K-means algorithm does not necessarily identify the most optimal configuration in terms of the global objective function minimum. The algorithm is also significantly sensitive to the initial randomly selected cluster centres. However, the K-means algorithm can be run multiple times to reduce this effect.

2.3.2 Fuzzy c-means algorithm

The Fuzzy c-Means clustering algorithm (FCM) was initially developed by Dunn (1973) and later generalised by Bezdek (1981). This algorithm is based on optimising the objective function given by Equation (6)

$$J_{fcm}(Z; U; V) = \sum_{i=1}^c \sum_{k=1}^N (\mu_{ik})^m \|z_k - v_i\|^2, \quad (6)$$

where the matrix $U = [\mu_{ik}] \in M_{fmc}$ is a fuzzy partition of Z , and $V = [v_1, v_2, \dots, v_c]$ is the vector of prototypes of the clusters, which are calculated according to $D_{ikA_i} = \|z_k - v_i\|^2$, which is a square inner-product distance norm. $m \in [1, \infty]$ is a weighting exponent that determines the fuzziness of the resulting clusters. The optimal partition U^* of Z using the Fuzzy c-Means

1 algorithm is reached by implementing the couple (U^*, V^*) to locally minimise the objective
 2 function J_{fmc} according to an alternating optimisation method (Ojeda-Magaña, 2009).

3

4 Theorem FMC: If $D_{ikA_i} = \|z_k - v_i\| > 0$ for every $i, k, m > 1$ and Z containing at least c different
 5 patterns, $(U, V) \in M_{fmc} \times \mathfrak{R}^{c \times N}$ and J_{fmc} can be minimised only if

$$6 \quad \mu_{ik} = \left(\sum_{j=1}^c \left(\frac{D_{ikA_i}}{D_{jkA_i}} \right)^{2/(m-1)} \right)^{-1} \quad 1 \leq i \leq c ; 1 \leq k \leq n \quad (7)$$

7

$$8 \quad v_i = \frac{\sum_{k=1}^N \mu_{ik}^m z^k}{\sum_{k=1}^N \mu_{ik}^m} \quad 1 \leq i \leq c \quad (8)$$

9 Following the Eq. (7) and Eq. (8) presented above with respect to the FCM algorithm, given
 10 Z , choose the number of clusters $1 \leq i \leq N$, the weighting exponent $m > 1$ and, the ending
 11 tolerance $\delta > 0$. Then, the solution can be reached with the following steps:

- 12 • Provide an initial value to each one of the prototypes v_i , $i = 1, \dots, c$. These values are
 13 generally generated randomly.
- 14 • Calculate the distance of patterns z_k from each of the i th prototypes v_i using
 15 $D_{ikA_i}^2 = (Z_k - v_i)^T A_i (z_k - v_i)$, $1 \leq i \leq c$, $1 \leq k \leq N$.
- 16 • Determine the membership degrees of the matrix $U = [\mu_{ik}]$, if $D_{ikA_i} > 0$ using Eq. (6).
- 17 • Calculate the new values of the prototypes v_i using Eq. (7).
- 18 • Verify if the error is greater than δ . If it is, move on to the second step. Otherwise,
 19 stop.

20

21

22

1 **2.3.3 Self Organising Maps**

2 An artificial Neural Network (ANN) is a mathematical model that attempts to simulate the
3 structural and functional aspects of biological neural networks. ANN can be classified as both
4 supervised and unsupervised. The most important features that relate to an ANN with respect
5 to biological neural networks are that knowledge is acquired through a learning process, and
6 synaptic weights are used to store knowledge (Haykin, 1998). ANNs are considered very
7 powerful classifiers compared to classical algorithms. The algorithms used in ANN
8 applications are capable of finding good classifiers based on a limited and generally small
9 number of training examples. This capability, also referred to as generalisation, is useful from
10 a pattern recognition standpoint since a large set of parameters is estimated using a relatively
11 small data set.

12

13 Self Organising Maps (SOM) are a type of unsupervised learning tool used for the goal of
14 discovering the underlying structure of data. A topological map is simply a mapping that
15 preserves neighbourhood relations, and it consists of a set of units that are arranged in a
16 certain topology. SOM basically provide a form of cluster analysis by producing a mapping of
17 high-dimensional input data X , $X \in \mathfrak{R}^n$, in the output space while preserving the topological
18 relationship between the input data items as faithfully as possible. Each of the units i is
19 assigned a weight vector m_i of the same dimension as the input data, where $m_i \in \mathfrak{R}^n$. In the
20 initial setup of the model prior to training, the weight vector is filled with random values.
21 During the learning step, the unit c with the highest activity level, which is the winner c with
22 respect to a randomly selected input pattern x , is adapted in a way that will allow it to exhibit
23 an even higher activity level at future presentations of that specific input pattern. Commonly,
24 the activity level of a unit is based on the Euclidian distance between the input pattern and the
25 pattern weight unit of that vector. The unit showing the lowest Euclidean distance between its
26 weight vector and the current input vector is selected as the winner. Hence, the selection or
27 winner c may be written as follows:

$$28 \quad c : \|x - m_c\| = \min_i \|x - m_i\| \quad (9)$$

29

1 Adaptation takes place at each learning iteration and is performed as a gradual reduction of
2 the difference between the respective components of the input vector and the weight vector.
3 The amount of adaptation is guided by the learning rate α , which gradually decreases over
4 time. As an extension to standard competitive learning, units in a time-varying and gradually
5 decreasing neighbourhood surrounding the winner are adapted. This strategy enables the
6 formation of large clusters in the beginning and fine-grained input discrimination toward the
7 end of the learning process. In combining these principles of SOM training, we may write the
8 learning rule as given in Equation (10):

$$9 \quad m_i(t+1) = m_i(t) + \alpha(t)h_{c_i}[x(t) - m_i(t)], \quad (10)$$

10 where t denotes the current learning iteration, and α represents the time-varying learning
11 rate. c_i represents the time-varying neighbourhood kernel, and x represents the current input
12 pattern. Finally, m_i denotes the weight vector assigned to unit i .

13

14 **2.4 Classification**

15 Classification is one of the most frequently encountered decision-making tasks in human
16 activity. A classification problem occurs when an object needs to be assigned to a predefined
17 group or class based on a number of observed attributes related to that object. In this case, we
18 must classify soil images in two classes, one representing soil and the other representing pore
19 space.

20

21 An ANN was used to classify soil images into two classes (pore space and solid soil). ANN is
22 characterised by a great degree of modularity and flexibility, also it is very efficient for
23 demanding large-scale and generic pattern recognition applications.

24

25 **2.4.1 Feed Forward Neural Network**

26 Feed Forward Neural Network (FFNN), also known as multilayer perceptrons (MLP), are
27 popularly used in many practical applications. FFNN is a type of supervised learning.
28 Knowledge is acquired by the network through a learning process known as the Back
29 Propagation (BP) algorithm. The BP algorithm serves as a workhorse in the design of a

1 special class of layered FFNN. A FFNN has an input layer of source nodes and an output
2 layer of neurons; these two layers connect the network to the outside world. In addition to
3 these two layers, the multilayer perceptron usually has one or more layers of hidden neurons,
4 which are called hidden because they are not directly accessible. The hidden neurons extract
5 important features contained in the input data. Using supervised learning, these networks can
6 learn the mapping from one data space to other examples. The term BP refers to the way in
7 which the error is computed at the output side. Namely, it is propagated backwards from the
8 output layer to the hidden layer and finally to the output layer; details on this method can be
9 found in Basheer (2000).

10

11 Three FFNN with the same structure were tested, one for each segmentation method. The
12 network structures used are as follows:

- 13 • Input layer: four neurons, where each neuron is an image feature.
- 14 • Hidden layer: one hidden layer with ten neurons.
- 15 • Output layer: one output layer, where in the output layer two classes are obtained.
- 16 • Learning rate: 1
- 17 • The used activation function: the log-sigmoid function.
- 18 • Training set: eight images, two for each horizon.
- 19 • Training conditions: epoch = 250.
- 20 • Performance function: Mean Squared Error (MSE) = 0.01.
- 21 • Test set: four images, an image for each horizon.

22 All mathematical computations were performed using Matlab®.

23

24 **3 Results and discussion**

25 **3.1 Feature extraction**

26 For each studied image, we applied an erosion morphological operation to enhance the dark
27 regions (that is, pore space). The structuring element will darken the image. Bright regions
28 surrounded by dark regions (pore space) shrink in size, and dark regions surrounded by bright

1 regions (that is, soil solid) grow in size. Small, bright pixels in images will disappear as they
2 are eroded down to the surrounding intensity value, and small dark pixels will become larger
3 pixels. The effect is most marked at places in the image where intensity changes rapidly,
4 whereas regions with fairly uniform intensity will be left more or less unchanged, except at
5 their edges. A cross-shaped structuring element of 3×3 size window was applied. Fig. 2
6 shows the results for a given image. Fig. 2(a) shows grey-scale CT soil images. Fig. 2(b)
7 depicts the results after a morphological erosion operation.

8

9 In this work, we applied two window-based features, namely, mean and standard deviation;
10 they were extracted from eroded images within a rectangular window. Two windows of
11 different sizes were applied. The correlation analysis was implemented to find the best pixel
12 block window according to the results already obtained; as such, we chose a 5×5 pixel
13 window.

14

15 **3.2 Image segmentation**

16 Three clustering methods were implemented to obtain segmented images. We built a FV,
17 $S_s = \{x^{(qs)} : q_s = 1, \dots, Q_s\}$, where $x^{(qs)} \in \mathfrak{R}^D$ is a D-dimensional vector, and Q_s is the number
18 of pixels in the image, where $x^{(qs)} = \{[x_1^{(qs)}, x_2^{(qs)}, x_3^{(qs)}, x_4^{(qs)}]\}$. The FV set is then clustered
19 using three different methods.

20

21 S_s are grouped into k clusters, where only one group corresponds to pore space, and the others
22 correspond to different types of soil solid. Various approaches are used to determine which
23 cluster represents the pore group, including the minimum percentage of total data and the
24 minimum grey level of the original image. The remaining clusters represent soil group. The
25 previous clustering results are represented as a segmented image of binary form, where 0
26 value corresponds to a pore space class and 1 value corresponds to a soil solid class. Next, we
27 show the initial conditions for segmentation and the results of each clustering method.

28 **3.2.1 K-means**

29 The initial conditions for this method were as follows.

- 1 - The cluster number took values from 7 to 11.
- 2 - Centroids were initialised as random values.
- 3 - The Euclidean distance function was used to measure distance.
- 4 - The maximum iteration number was set at 100.

5 To illustrate the results, Fig. 3 shows the segmented image and the binary image obtained by
6 applying the K-means algorithm.

7

8 **3.2.2 FCM**

9 The initial conditions for this method were as follows:

- 10 - The cluster number took values from 7 to 11.
- 11 - Centroids were initialised as random values.
- 12 - The number of membership degrees was set to 2.
- 13 - The maximum number of iterations was set to 100.
- 14 - The minimum amount of improvement was set to 1e-3.

15

16 To illustrate the results, Fig. 4 shows the segmented and binary images obtained by applying
17 FCM algorithm.

18 **3.2.3 SOM**

19 The initial conditions for this method were as follows:

- 20 - The network structure [4 k] was such that k took values from 7 to 11.
- 21 - The weight vector was randomly initialised.
- 22 - The topology function was hextop.
- 23 - The distance function was linkdist.
- 24 - The maximum epoch was set at 100.

25

1 To illustrate these results, Fig. 5 shows the segmented and binary images obtained by
2 applying SOM.

3

4 The group corresponding to the pore class was obtained under the following conditions.

5 The data were clustered into several groups, the number of which ranged from 7 to 11; the
6 percentage that corresponded to pore space was then computed. The obtained percentages in
7 this work were compared with the results obtained by Piñuela et al. (2009), who used the
8 threshold method. Taking into account their results, we chose a number of groups equal to 9.
9 Table 2 shows the porosity percentage from Piñuela et al. (2009). Table 3 shows the
10 percentage of pore space obtained using our method. Based on this comparison, the FV was
11 clustered and labelled into nine groups. These labelled vectors were then used for
12 classification.

13

14 **3.2.4 Pore Space Distribution**

15 In this study, we observed that it is not only the percentage of porosity that influences the
16 threshold method; in addition, certain pore sizes present a higher influence, as is shown in
17 Fig. 6. Pores with sizes ranging from 50 pixels to 400 FCM and K-means show a similar
18 accumulative porosity curve; meanwhile, SOM shows a lower increase. For pores that are
19 greater than 400 pixels, the accumulative curves decrease until the pore size reaches 2000
20 pixels under the FCM and -means algorithms. However, in terms of total porosity, this may
21 not be significant, especially considering the substantial influence of hydraulic simulation and
22 behaviour.

23 **3.3 Image classification**

24 We used 2D CT soil images to detect the percentage of pore space in soil. The image
25 resolution is 45.1 μm , and the image size is 256x256 pixels, so that we have 65,536-pixels by
26 image. We built a FV from the set S_s , which includes 786,432 feature vectors obtained from
27 feature extraction (pixels corresponding to twelve images). Then, we clustered and labelled
28 FV into the set S_s using the K-means, FCM and SOM algorithms to compare results. Each

1 FV was partitioned into two sets, namely, a training set with 524,288 feature vectors and a
2 test set with 262,144 feature vectors.

3 The classification results are represented by the output vector (V_{out}). Three FFNNs were used
4 for training and testing with the same conditions to compare classification results.

5

6 Classification was performed for each FV obtained in the clustering step. Table 4 shows the
7 results of the classification for each FV (test set). According to the obtained results, the best
8 classification rate was obtained using the FV for the K-means algorithm.

9

10 **3.3.1 Image reconstruction**

11 V_{out} contains the classification results, where V_{out} is formed by two classes, with one
12 corresponding to solid soil and the other corresponding to pore space. Using V_{out} , we built
13 four images and computed the pore percentage for each reconstructed image. These results are
14 compared with the obtained percentage in Table 3.

15

16 Table 5 shows the comparison results, where the initial percentage obtained in the segmented
17 images is compared with the classifier output. Fig. 7 shows the reconstructed image for each

18 V_{out}

19

20 **4 Conclusions**

21 This paper proposed an alternative way to detect pore space in CT soil images using image
22 processing, data clustering and ANN. Feature extraction in soil images is an important factor
23 for the pore space detection due to the low level of contrast in these image types. We applied
24 an erosion morphological operation to enhance the dark regions (pore space); in addition, the
25 mean and standard deviation were used to generate additional information about areas of
26 interest.

27

28 Clustering algorithms help us to get a better comprehension and knowledge of data with the
29 objective of segmented image into different areas according to given objectives. After a

1 learning process, the partitional clustering algorithms provide a set of centroids as the most
2 representative elements of each group. As such, clustering algorithms partition the input
3 images in homogeneous areas, each of which is considered homogeneous with respect to a
4 property of interest.

5

6 Unlike image segmentation based on histograms, this method allows a deeper analysis of the
7 areas where the pore and soil are mixed because segmentation by clustering facilitates the
8 analysis of multidimensional data, while segmentation using histogram analysis allows us to
9 analyse only one dimension.

10

11 In this work, we proposed an ANN as a classifier. ANN has been used with success in
12 different investigation fields. This classifier plays an important role in our methodology
13 because ANN can learn structure in data through examples contained in a training set and
14 then can conduct complex decision making. Our methodology provides an alternative way to
15 detect solid soil and pore space in CT images. The percentages of correct classifications of
16 pore space in images were 97.01%, 96.47 % and 96.12%.

17

18

19 **Acknowledgements**

20 The authors wish to thank the National Council for Science and Technology (CONACyT), the
21 Secretariat of Public Education (SEP), the Government of Mexico and the Group of
22 Automation in Signal and Communications (GASC) of the Technical University of Madrid
23 for their contributions.

24

25

26

27

28

29

1 **References**

- 2 Arias, S., Gómez, H., Prieto, F., Botón, M., Ramos, R.: Satellite image classification by self
3 organized maps on GRID computing infrastructures, Proceedings of the second EELA-2
4 Conference, 1-11, 2009.
- 5 Basheer, I.A., Hajmeer, M.: Artificial neural networks fundamentals, computing, design, and
6 application, Journal of Microbiological methods 43, 3-31, 2000.
- 7 Bezdek, J. C.: Pattern Recognition with Fuzzy Objective Function Algorithms. Plenum Press,
8 New York, 1981
- 9 Capowiez, Y., A. Pierret, O. Daniel, M. P., A. Kretzschmar.: 3D skeleton reconstructions of
10 natural earthworm burrow systems using CAT scan images of soil cores. Biol. Fertil. Soils,
11 27, 51–59, 1998
- 12 Chuang, K.S., Tzeng, H.L., Chen, S., Wu, J., Che, T.J.: Fuzzy c-means clustering with spatial
13 information for image segmentation, Computerized medical imaging and graphics, 30, 9-15,
14 2006.
- 15 De Oliveira, L., Braz, G., Correa, A., Cardoso, A., Gattas, M.: Detection of masses in digital
16 mammograms using K-means and support vector machine, Electronic letters on computer
17 vision and images analysis, 8(2), 39-50, 2009
- 18 Dunn, J.C.: A Fuzzy relative of isodata process and its use in detecting compact well-
19 separated clusters, Journal of Cybernetics, 3, 32-57, 1973.
- 20 Gonzalez, R.C., Woods, R.E.: Digital image processing, Prentice Hall, 2002
- 21 Haykin,S., Neural Networks: A comprehensive foundation, Prentice Hall, 1999
- 22 Jian, Y., Zhou, Z.H.; SOM Ensemble-based image segmentation, Neural Processing Letters,
23 20, 171-178, 2004
- 24 MacQueen, J. B.: Some Methods for classification and Analysis of Multivariate
25 Observations, Proceedings of 5-th Berkeley Symposium on Mathematical Statistics and
26 Probability, Berkeley, University of California Press, 1, 281-297, 1967.
- 27 Melo, F.J.R., dos Santos, M.C.: Micromorfologia e mineralogía de dois solos de Tabuleiro
28 costeiro de Pernambuco, R. Bras.Ci. Solo, 20, 99-108, 1996.

- 1 Mermut, A.R.: Historical Development in soil micromorphological imaging. *J.Mt.Sci.*, 6,
2 107-112, 2009.
- 3 Ojeda-Magaña, B., Ruelas, R., Quintanilla-Dominguez, J., Andina, D.: Images sub-
4 segmentation by Fuzzy and possibilistic Clustering Algorithms, 100-109, 2009.
- 5 Pal, N.R., S.K. Pal.: A review of image segmentation techniques. *Patt. Recogn.*, 29, 1277–
6 1294. 1993
- 7 Perret, J.S., Prasher, S.O., Kacimov, A.R. :Mass fractal dimension of soils macropores using
8 computed tomography: from the box counting to the cube-counting algorithm, *Journal of*
9 *hydrology*, 267, 285-297, 2003.
- 10 Pal, N.R., Pal, S.K., Keller, J.M., Bezdek, J.C.: A possibilistic fuzzy c-means clustering
11 algorithm, *IEEE transactions on Fuzzy systems*, 13(4), 527-530, 2005.
- 12 Peth, S., Horn, R., Beckmann, F., Donath, T., Fischer, J., Smucker, A.J. M.:Three
13 Dimensional Quantification of intra-aggregate pore-space features using synchrotron-
14 radiation-based microtomography, *Sil.Sci. Soc. Am. J.*, 72, 897-907, 2008.
- 15 Piñuela, J., Alvarez, A. , Andina, D., Tarquis, A.M.: Quantify a soil pore distribution from 3D
16 images: Multifractal spectrum through wavelet approach. *Geoderma*, 155, 203-210, 2009.
- 17 Quintanilla-Dominguez, J., Cortina-Januchs, M.G., Barrón-Adame, J.M., Vega-Corona, A.,
18 Buendía-Buendía, F.S., Andina, D.: Detection of microcalcification using coordinate logic
19 filters and artificial neural networks. *LNCS*, 5602, 179-187, 2009.
- 20 Sofou, A., Evangelopoulos G., Maragos, P.: Soil Image Segmentation and Texture Analysis:
21 A Computer Vision Approach. *Geoscience and remote sensing letters*, 2(4), 394-398, 2005.
- 22 Tarquis, A.M., Heck R.J., Andina, A., Antón, J.M.: Pore network complexity and
23 thresholding of 3D soil images. *Ecological complexity*, 6, 230-239, 2009.
- 24 Vogel, H.J., Kretschmar A.: Topological characterization of pore space in soil-sample
25 preparation and digital image-processing, *Geoderma*, 73, 23-38, 1996.
- 26 Kohonen, T.: The self organizing map (SOM), *Proceedings of the IEEE*, 78(9), 1464-1480,
27 1990.
- 28 Lázaro, J., Arias, J., Martín, J.L., Zoloaga, A., Cuadrado, C.: SOM segmentation of gray scale
29 images for optical recognition, *Pattern recognition letters*, 27, 1991-1997, 2006.

1 Ye, Z.: Objective assessment of nonlinear segmentation approaches to gray level underwater
2 images, ICGST-GVIP journal, 9(2), 39-46, 2009.

3 Vega-Corona, A., Álvarez-Vellisco, A., Andina, D.: Feature vectors generation for detection
4 of microcalcification in digitized mammography using neural network, LNCS, 2687, 583-590,
5 2003.

6

7

8

9

10

11

12

13

14

15

16

17

18

19

20

21

22

23

24

25

26

1 Table 1. Physical properties of the selected horizons of Argissol according to Melo and Dos
2 Santos (1996).

Horizon	Depth (cm)	Particle size distribution (%)			
		C. Sand	F. Sand	Silt	Clay
A2	10-35	62	24	3	11
AB	35-57	26	53	4	17
Bt2	98-152	21	40	4	23
Bt/Bw	150-190	18	37	10	35

3
4
5
6
7
8
9
10
11
12
13
14
15
16
17
18
19
20

1 Table 2. Porosity percentages using thresholding criteria (Piñuela, 2009).

Horizon	Porosity (%)
A2	13.45
AB	14.73
Bt2	12.14
Bt/Bw	12.76

- 2
- 3
- 4
- 5
- 6
- 7
- 8
- 9
- 10
- 11
- 12
- 13
- 14
- 15
- 16
- 17
- 18
- 19
- 20
- 21

1 Table 3. The percentage of pore space obtained in clustering methods for each horizon, where
 2 the cluster number takes values ranging from 7 to 11.

No. of Clusters	K-Means (%)				Fuzzy C-Means (%)				SOM (%)			
	A2	AB	Bt2	Bt/Bw	A2	AB	Bt2	Bt/Bw	A2	AB	Bt2	Bt/Bw
7	19.60	18.00	14.13	16.94	18.11	16.80	13.86	15.96	20.44	18.52	17.46	18.66
8	16.72	15.17	13.35	13.42	15.54	13.79	11.87	13.34	17.79	15.89	14.77	16.02
9	13.57	11.86	11.98	12.06	13.32	11.70	10.46	11.61	15.59	13.83	12.77	13.95
10	11.92	10.15	10.11	11.98	11.49	10.00	.27	10.51	13.80	12.11	11.27	12.47
11	9.58	8.84	6.25	10.39	10.00	8.79	8.36	9.16	12.45	10.74	10.04	11.13

3
 4
 5
 6
 7
 8
 9
 10
 11
 12
 13
 14
 15
 16
 17
 18
 19
 20

1 Table 4. The classification percentages obtained for each FV.

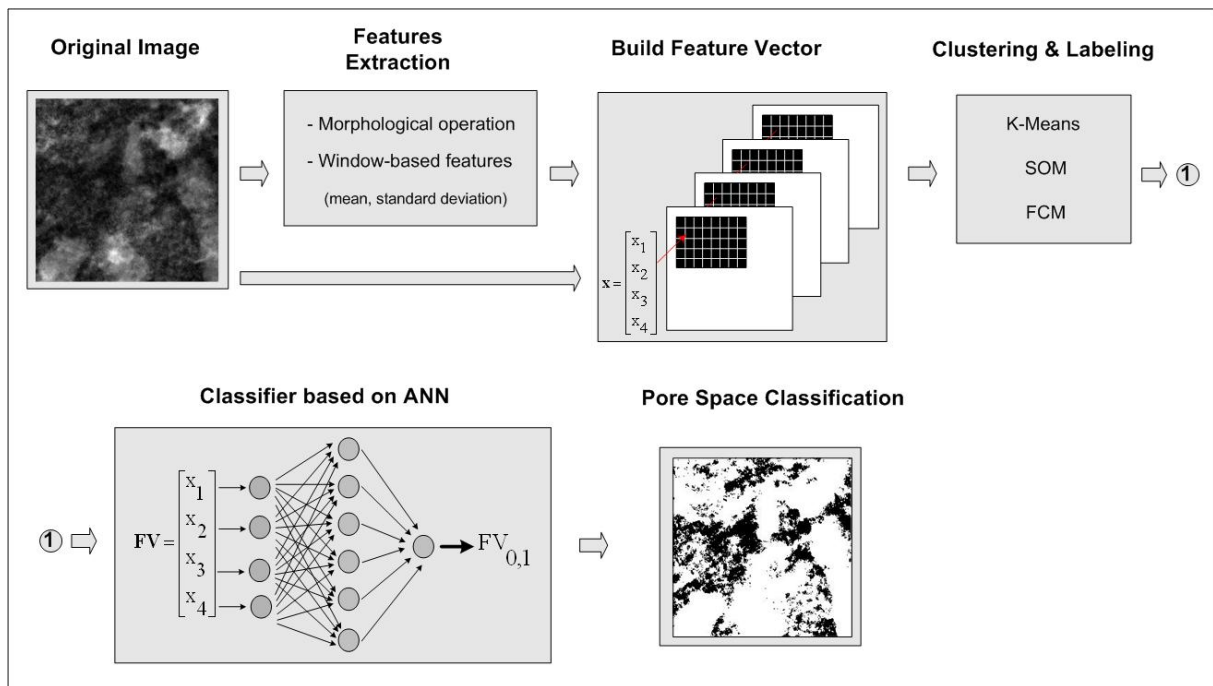
FV for clustering method	Correct classification (%)
K-means	97.01
FCM	96.44
SOM	96.12

2
3
4
5
6
7
8
9
10
11
12
13
14
15
16
17
18
19
20
21

1 Table 5. Porosity percentages for FFNN classifications.

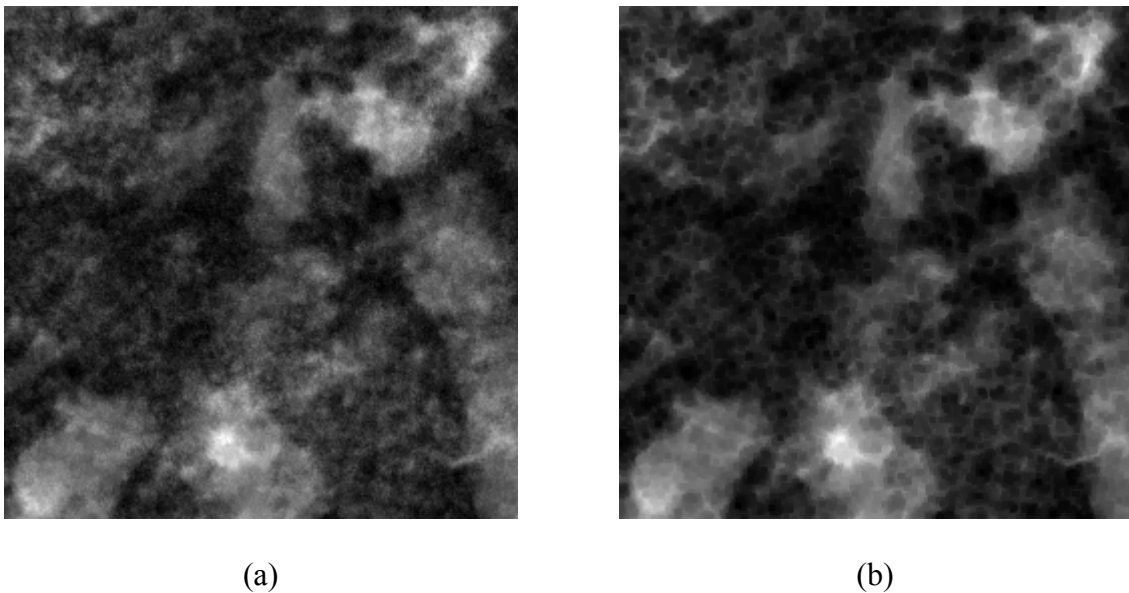
Horizon	K-Means (%)		Fuzzy C-Means (%)		SOM (%)	
	Initial percentage	Final percentage	Initial percentage	Final percentage	Initial percentage	Final percentage
A2	13.57	13.30	13.32	12.29	15.59	14.83
AB	11.86	3.45	11.70	3.03	13.83	3.98
Bt2	11.98	14.55	10.46	13.06	12.77	16.68
Bt/Bw	12.06	10.72	11.61	9.68	13.95	12.17

2
3
4
5
6
7
8
9
10
11
12
13
14
15
16
17
18
19



1
2
3
4
5

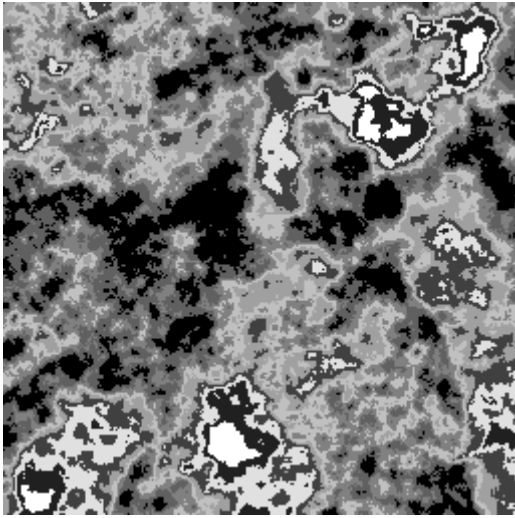
Figure 1. The block diagram of our proposed method.



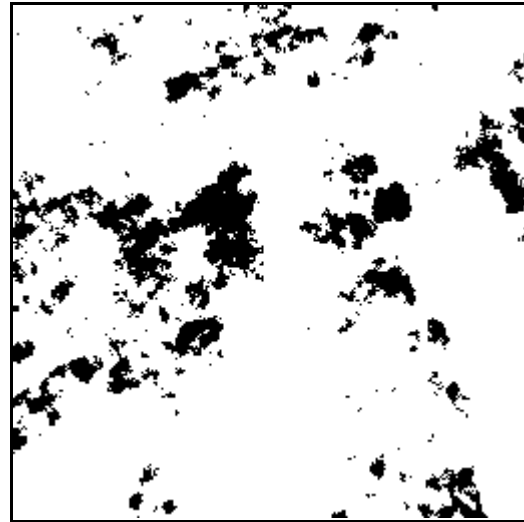
6 Figure 2. The obtained result for a soil image: (a) the CT soil image in grey scale; (b) the
7 results after a morphological erosion operation.
8

1

2



(a)



(b)

3 Figure 3. The obtained results for the K-means method: (a) the image segmented with nine
4 clusters; and (b) the binary image obtained from the segmentation process, where 0 value
5 corresponds to the pore space class and 1 value corresponds to the soil solid class.

6

7

8

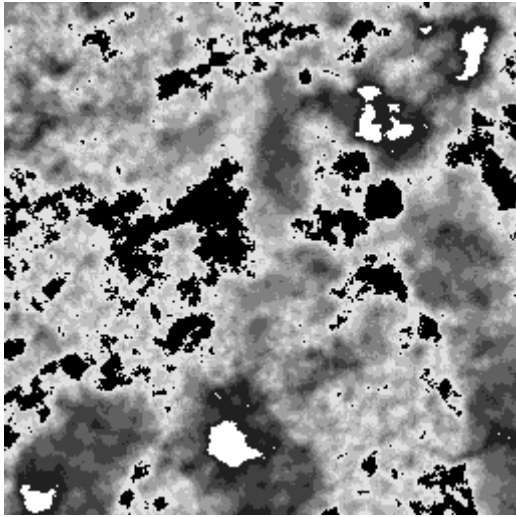
9

10

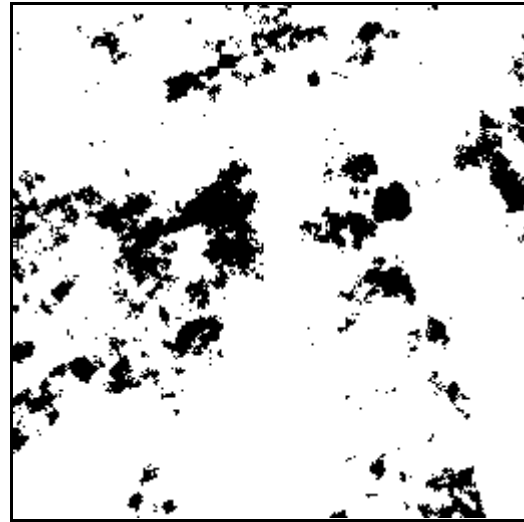
11

12

13



(a)

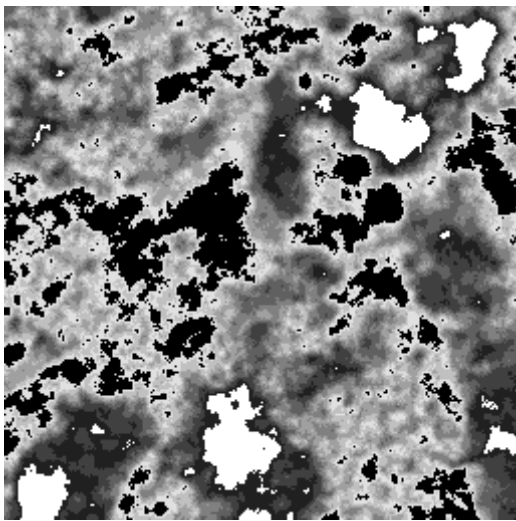


(b)

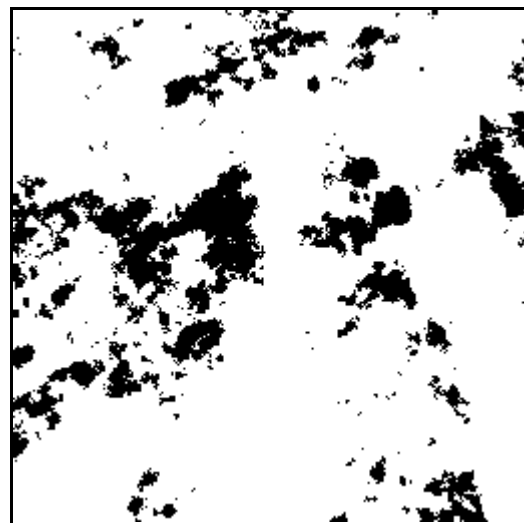
1 Figure 4. The obtained results for the Fuzzy c-means method: (a) the image segmented with
2 nine clusters; and (b) the binary image obtained from the segmentation process, where 0 value
3 corresponds to the pore space class and 1 value corresponds to the soil solid class.

4

5



(a)

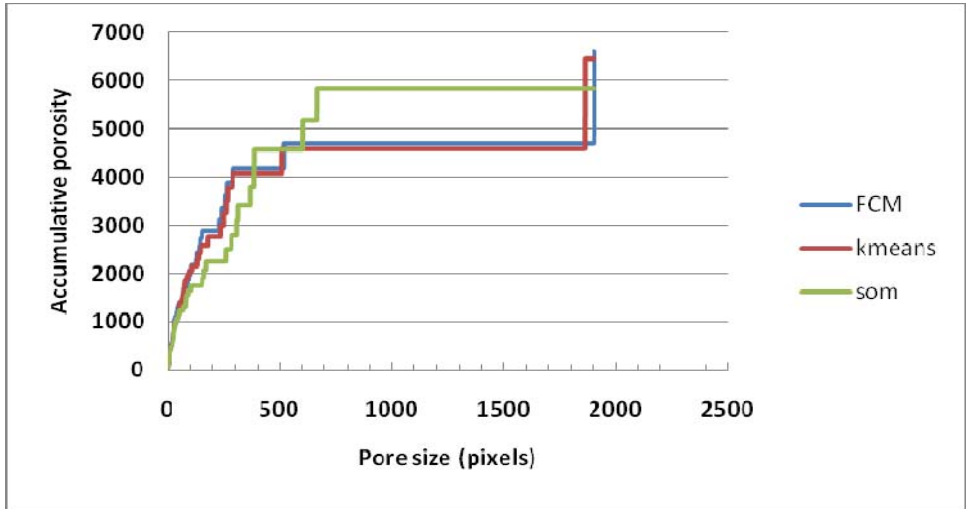


(b)

6 Figure 5. The obtained results for the SOM method: (a) the image segmented with nine
7 clusters; and (b) the binary image obtained from the segmentation process, where 0 value
8 corresponds to the pore space class and 1 value corresponds to the soil solid class.

9

1



2

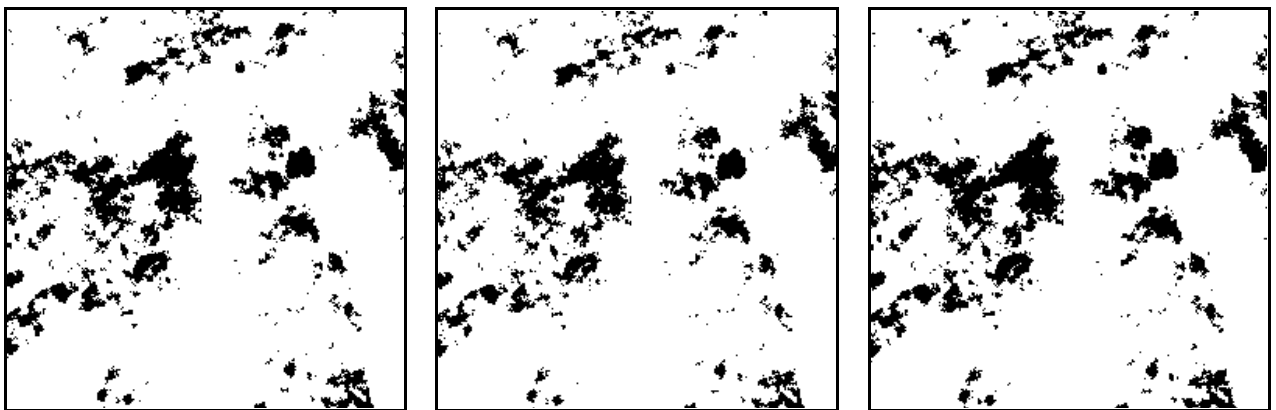
3

4 Figure 6. Pore space distribution for the A2 horizon.

5

6

7



(a)

(b)

(c)

8 Figure 7. The obtained classification results: (a) the classification obtained with the K-means
9 algorithm, where the image is segmented with nine clusters; and (b) the binary image
10 obtained from the segmentation process, where 0 value corresponds to the pore space class
11 and 1 value corresponds to the soil solid class.

12

13